Check for updates

New sustainable ternary copper phosphide thermoelectrics†

Robert J. Quinn, [a] Callum Stevens, [b] Hector Leong,[b] Andrew D. Huxley[b] and Jan-Willem G. Bos *[a]

The thermoelectric performance of ACuP (A = Mg and Ca) with abundant elements and low gravimetric density is reported. Both systems are p-type doped by intrinsic Cu vacancy defects, have large power factors and promising figures of merit, reaching $zT = 0.5$ at 800 K. This demonstrates that copper phosphides are a potential new class of thermoelectric materials for waste heat harvesting.

Thermoelectric generation is a promising source of renewable energy that uses a temperature gradient to produce power. Despite the obvious attraction of converting waste heat into useful electricity, widespread application has been hindered by the absence of cost-effective thermoelectric materials.[1,2]

The efficiency of a thermoelectric material increases with its figure of merit, $zT = (S^2/\rho\kappa)T$. Here, S is the Seebeck coefficient (voltage response to a temperature gradient), ρ is the electrical resistivity, κ is the thermal conductivity, which has electronic (κ_e) and lattice vibration (κ_{lat}) components, and T is the absolute temperature.

Here, we present the thermoelectric properties of two promising ACuP (A = Mg, Ca) copper phosphide materials. These unexplored compositions reach figures of merit, $zT = 0.5$ at 800 K and have peak power factors, $S^2/\rho = 1.5–1.75$ mW m^{-1} K^{-2}, suited to power generation from waste heat. Dense disks are stable on the bench in ambient conditions and show reproducible cycling performance up to 800 K under a He atmosphere. Mg, Ca, Cu and P are all abundant elements making the ACuP phosphides a more sustainable choice than Bi, Pb and Te containing thermoelectric materials. Another beneficial feature is the low gravimetric densities of 4.3 g cm^{-3} (A = Mg) and 4.0 g cm^{-3} (A = Ca). This is comparable to the low-weight thermoelectric Mg$_2$(Si/Sn)

alloys (2–3.5 g cm^{-3}) and much lower than Bi$_2$Te$_3$ (7.7 g cm^{-3}), PbTe (8.2 g cm^{-3}) or intermetallic compositions.

Metal phosphides are currently attracting wider interest as potential thermoelectric materials,[3] inspired by the success of Zintl phases based on Sb,[4] and the realisation that despite the low atomic mass of P, complex crystal structures can still have low κ_{lat}, while small electronegativity differences support good electrical properties. Recently investigated phosphides include cage-like tetrahedrite Ag$_6$Ge$_{10}$P$_{12}$ with $zT = 0.7$ at 750 K,[5,6] layered CaZn$_2$P$_2$ and YbCuZnP$_2$ materials with $zT = 0.6$ at 973 K for YbCuZnP$_2$,[7–9] the clathrate Ba$_8$Cu$_{14}$Ge$_6$P$_{26}$ with $zT = 0.6$ at 800 K,[10] Zn$_{1-x}$Cu$_2$P$_8$ with $zT = 0.25$ at 673 K,[11] and tetragonal Cd$_3$P$_2$ with $zT = 0.9$ at 673 K.[12,13] We have recently reported a related silver phosphide, CaAg$_{1-x}$P ($x = 0.1$), containing corner- and edge-sharing AgP$_5$ square pyramids, achieving a highest $zT = 0.4$ at 800 K.[14]

The crystal structures of MgCuP and CaCuP are illustrated in Fig. 1 and are both distinct from CaAg$_{1-x}$P. MgCuP is orthorhombic (space group *Pnma*) and has a structure consisting of CuP$_4$ tetrahedra and MgP$_5$ square pyramids linked by corner and edge sharing.[15] Both tetrahedra and square pyramids are distorted from their ideal geometries. In the *b* direction, the
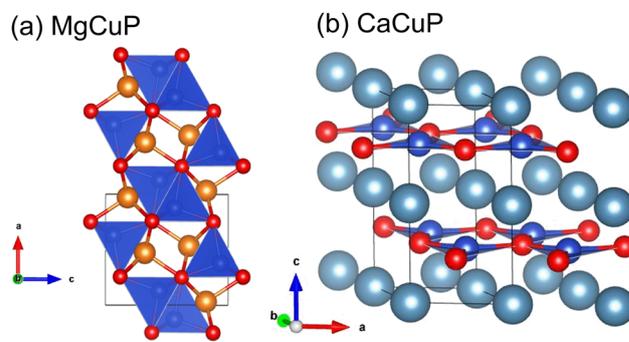

Fig. 1 Crystal structures of (a) MgCuP and (b) CaCuP. Mg = orange, Ca = turquoise, Cu = blue and P = red. In MgCuP, edge linked CuP$_4$ tetrahedra form chains aligned in the *b* direction.

[a] Institute of Chemical Sciences and Centre for Energy Storage and Recovery, School of Engineering and Physical Sciences, Heriot-Watt University, Edinburgh, EH14 4AS, UK. E-mail: j.w.g.bos@hw.ac.uk

[b] SUPA School of Physics and Astronomy, University of Edinburgh, Edinburgh, EH9 3FD, UK

CuP_4 tetrahedra are linked by edge sharing, while in the a and c directions only corner sharing is present. This gives rise to quasi 1D copper phosphide chains (Fig. 1a) with short Cu–Cu bond distance ~ 2.70 Å, comparable to ~ 2.54 Å in elemental Cu. This difference in connectivity is reflected in the calculated bandstructure with dispersive electronic bands along the chain direction and flat bands in the other directions.[17] CaCuP has a layered hexagonal structure (space group $P6_3/mmc$) consisting of $[CuP]^{2-}$ graphene-like layers separated by Ca^{2+} cations.[16] Electronic structure calculations show dispersive bands within the $[CuP]^{2-}$ planes, with flatter bands for transport across the Ca^{2+} layers.[17] Both compositions have comparable calculated indirect electronic bandgaps, $E_g = 1.1$–1.2 eV.[17]

Successful synthesis (protocol is outlined in the ESI†) of these samples was confirmed by X-ray powder diffraction. Rietveld fits are shown in Fig. S1 (ESI†), and the main crystallographic data is summarised in Table S1 (ESI†). Both samples contain low levels of impurities. In case of MgCuP, Cu_3P (~ 3 wt%) and CuP_2 (~ 0.8 wt%) were identified as impurity phases. For CaCuP, ~ 3 wt% of the trigonal form of $CaCu_4P_2$[18] is observed alongside a second very small weight fraction of unidentified impurity. As shown below, both materials are p-type semiconductors with high levels of doping. Most commonly this is caused by small transition metal deficiencies.[14] Rietveld fitting of site occupancies confirms the presence of small $<1\%$ deficiencies on the Cu-site, while the Mg/Ca and P sites are stoichiometric (Table S1, ESI†). Diffraction measurements and SEM on fractured surfaces of the hot-pressed disks did not show any evidence for texturing (Fig. S2 and S3, ESI†).

The thermoelectric properties of ACuP are shown in Fig. 2. Both samples have a positive $S(T)$ indicating p-type conduction (Fig. 2a). The linear temperature dependence reveals high levels of doping and degenerate semiconducting behaviour. Above 670 K, $S(T)$ for MgCuP begins to decrease, suggesting the emergence of n-type carriers.[19] These reduce $S = (\sigma_p S_p + \sigma_n S_n)/\sigma$, through the opposing sign of the hole and electron Seebeck coefficients, $S_{p/n}$. Here, $\sigma_{p/n}$ are the p-type and n-type contributions to the electronic conductivity $\sigma = 1/\rho$. The observation of n-type carrier effects above 670 K is unexpected given the large $E_g = 1.1$ eV from DFT calculations.[17] Application of the Goldsmid-Sharp model, $E_g = 2eS_{max}T_{max}$,[20] yields a thermal bandgap, $E_g = 0.22$ eV. This low value could indicate the presence of in-gap states that reduce the effective bandgap. However, the absence of substantial amounts of defects from Rietveld analysis suggests that this is not likely. A large difference between hole and electron mass can also serve to bring the Goldsmid–Sharp and DFT values in line.[21] $\rho(T)$ increases up to 670 K for both samples and up to the highest measured temperature for CaCuP (Fig. 2b), consistent with highly doped metal-like degenerate semiconducting behaviour. The decrease in $\rho(T)$ for MgCuP above 670 K is consistent with the emergence of n-type carriers, increasing the total conductivity $\sigma = \sigma_p + \sigma_n$.[19] $\rho(T)$ for MgCuP is over double that of CaCuP in the degenerate regime. For this reason the power factor, S^2/ρ of CaCuP is larger over the whole temperature range, as shown in Fig. 2c. The lower $\rho(T)$ of CaCuP contributes to a larger thermal conductivity
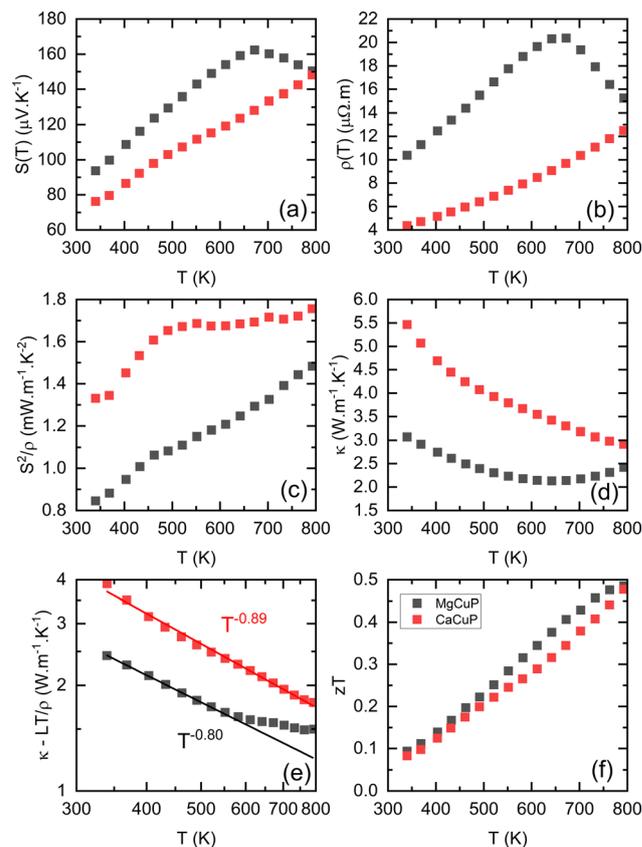

Fig. 2 Temperature dependence of (a) $S(T)$, (b) $\rho(T)$, (c) $S^2/\rho(T)$, (d) $\kappa(T)$, (e) $\kappa_{lat}(T)$ and (f) the figure of merit, zT for MgCuP (black) and CaCuP (red) between 300–800 K.

$\kappa(T)$ due to a larger electronic contribution $\kappa_{el} = LT/\rho$ (Fig. 2d). Here, L is the Lorenz number which is estimated from $S(T)$ using an empirical relation.[22] For MgCuP, $\kappa(T)$ increases rapidly above 670 K due to the presence of both p- and n-type carriers, resulting in a bipolar contribution $\kappa_{bi} = \sigma_p \sigma_n (S_p - S_n)^2 T/\sigma$.[23] This effect only occurs for materials with hole and electron currents in a thermal gradient and is linked to heat generated from recombination.[23] The κ_{lat} shown in Fig. 2e (log–log scale) was estimated by subtracting κ_{el}, which gives a good estimate in the single carrier regime. At 340 K, CaCuP has a substantially larger $\kappa_{lat} = 3.9$ W m^{-1} K^{-1} compared to 2.5 W m^{-1} K^{-1} for MgCuP. Both samples have a $\kappa_{lat} \sim T^{-q}$ dependence. Here, $q = 1$ is expected for defect-free crystalline materials, $q = 0.5$ is typical of alloyed systems, whilst glasses have $q < 0$.[23] The fitted exponents $q = 0.9$ (A = Ca) and $q = 0.8$ (A = Mg) are indicative of low levels of structural disorder, consistent with the nearly stoichiometric ACuP composition from Rietveld analysis. With increasing temperature, both samples attain similar $\kappa - \kappa_{el}$, which is due to the emergence of κ_{bi} for MgCuP. The differences in electronic and thermal transport largely end up cancelling each other out, with zT of both samples being quite similar as shown in Fig. 2f, increasing from $zT_{340K} = 0.1$ to $zT_{790K} = 0.5$. Extrapolating to higher temperatures, zT for CaCuP will continue to increase while MgCuP would inevitably decrease due to n-type carrier effects.

A possible explanation for the observation of n-type carrier effects in MgCuP is found in the heat-cool cycling in the electrical property measurements. MgCuP shows an unusual stable hysteretic effect where $S(T)$ and $\rho(T)$ are substantially reduced between 550–800 K on cooling (Fig. S4, ESI†). This suppression does not affect $S^2/\rho(T)$, which is identical for the heat-cool runs. The sample did not lose mass or discolour and post measurement X-ray diffraction yielded an unchanged pattern. However, a MgCuP bar quenched from 800 K during measurement showed increased amounts of Cu_3P (from 3 wt% to 7 wt%) and CuP_2 (from 0.8 wt% to 6 wt%). This suggests that a reversible phase transition of MgCuP into Cu–P and Mg–P phases occurs, with quenching trapping more of the binary phases. The presence of increasing amounts of Cu/Mg–P at high temperature provides a possible route to electron doping *via* insertion from impurity phases,[24] rather than from thermal excitations across the bandgap. Whilst the available data does not allow a firm statement to be made, the insertion scenario would explain the presence of a substantial n-type carrier effect at modest temperatures in a largely defect-free material with a large >1 eV bandgap.

To gain insight into the underlying electronic structure of the ACuP materials Hall measurements were carried out as described in the ESI† (Fig. S5 and S6). Both compositions have constant Hall carrier concentrations (n_H) between 10–300 K (Fig. 3), as expected for degenerate semiconductors. The obtained values are $n_H = 2.4 \times 10^{20}$ cm^{-3} (A = Mg) and $n_H = 1.6 \times 10^{20}$ cm^{-3} (A = Ca). This corresponds to Cu vacancy concentrations of $\sim 1\%$ assuming a single $4s^1$ electron is removed per Cu. This is in line with the diffraction results that indicate a slight deficiency on the Cu-site. A recent report on thin-film CaCuP has a similar $n_H \sim 1.2 \times 10^{20}$ cm^{-3}, but a lower $\mu_H \sim 36$ cm^2 V^{-1} s^{-1} compared to 100 cm^2 V^{-1} s^{-1} in this work.[25]

Density of states effective mass, $m_{DoS}^* = N_v^{\frac{2}{3}} m_b^*$ values were determined using the single parabolic band (SPB) model.[26] m_{DoS}^* is an important fundamental electronic parameter that determines the magnitude of S and is linked to the total orbital

and valley degeneracy (N_v) and band mass (m_b^*) of the carriers. The obtained values are $m_{DoS}^* = 1.7 m_e$ (A = Mg) and $m_{DoS}^* = 1.0 m_e$ (A = Ca). The larger m_{DoS}^* for MgCuP is consistent with the published bandstructure.[17] MgCuP has a single band at the valence band maximum (VBM), which occurs at the Γ-point ($N_v = 1$). Using the published anisotropic band masses $m_{\Gamma-x/z}^* = 6.3 m_e$ and $m_{\Gamma-Y}^* = 0.15 m_e$, yields $m_b^* = 1.8 m_e$. This average value is in good agreement with $m_b^* = 1.7 m_e$ from the SPB model. For CaCuP, the VBM also occurs at the Γ-point but there are two bands present ($N_v = 2$).[17] The experimental $m_b^* = 0.63 m_e$ is therefore much lower than the value for MgCuP. Using the published $m_{\Gamma-M/K}^*$ and $m_{\Gamma-A}^*$ values,[17] yields $m_b^* = 0.2 m_e$ and $m_b^* = 0.4 m_e$. These low values are in line with the low SPB value, confirming that the holes are indeed much lighter in CaCuP.

The heavier hole mass for MgCuP is reflected in the mobility with $\mu_H = 29$ cm^2 V^{-1} s^{-1} compared to $\mu_H = 101$ cm^2 V^{-1} s^{-1} for CaCuP. Ultimately the higher μ_H for CaCuP leads to overall better electronic properties, evidenced by the much larger S^2/ρ (Fig. 2c). The better electronic properties are confirmed by the weighted mobility, $\mu_W = (m_{DoS}^*/m_e)^{\frac{3}{2}} \mu_0$, which can be readily calculated from the measured $S(T)$ and $\rho(T)$ and is shown in Fig. S7 (ESI†).[27] Here, μ_0 is the mobility in the semiconducting limit ($n_H \rightarrow 0$). Using the m_{DoS}^* values from the SPB analysis yields $\mu_0 = 45$ cm^2 V^{-1} s^{-1} (A = Mg) and $\mu_0 = 180$ cm^2 V^{-1} s^{-1} (A = Ca) at 350 K. Hence, the hole mobility is 4 times higher in CaCuP. This large hole mobility leads to S^2/ρ that are leading amongst phosphide thermoelectrics. Fig. 4 shows a comparison of the temperature-averaged power factor $\langle S^2/\rho \rangle$ over a 340–670 K gradient for the current best thermoelectric phosphides. MgCuP and many of the other high zT materials have $\langle S^2/\rho \rangle \approx 1$ mW m^{-1} K^{-2}, whereas CaCuP approaches 2 mW m^{-1} K^{-2}. The high hole mobility for CaCuP may also be linked to the negative magnetoresistance (MR) that is observed for this compound (Fig. S5, ESI†). This is largely temperature-independent, reaching values up to -15% in 1 T. The observation of negative MR is unusual for non-magnetic semiconductors. Large MR up to high temperatures has been linked
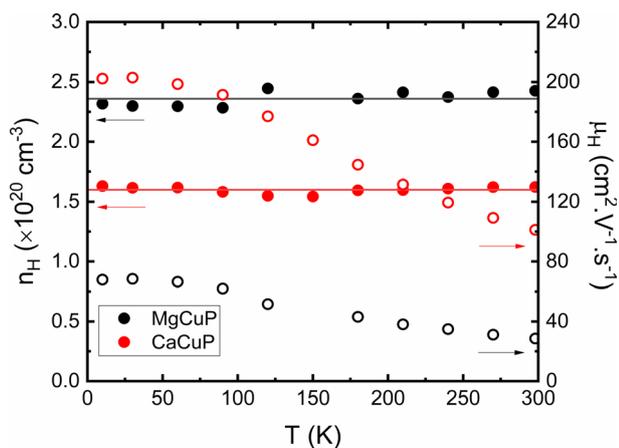
Fig. 3 The Hall carrier concentration (n_H) and mobility (μ_H) between 10–298 K, demonstrating that the hole concentration is independent of temperature.
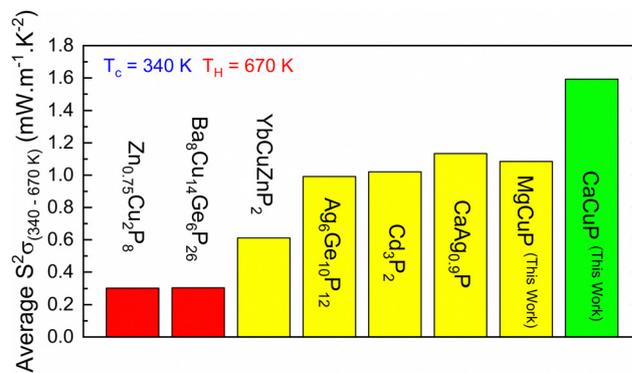
Fig. 4 Overview of temperature-average power factor $\langle S^2/\rho \rangle$ for leading metal phosphide thermoelectrics. Data taken from: $Zn_{0.75}Cu_2P_8$;[11] $Ba_8Cu_{14}Ge_6P_{26}$;[10] $YbCuZnP_2$;[8] $Ag_6Ge_{10}P_{12}$;[6] Cd_3P_2;[13] $CaAg_{0.9}P$.[14]

to topological electronic states in the Weyl semimetal TaP,[28,29] but the symmetry of CaCuP precludes these exotic topological effects.

To conclude, we report the thermoelectric properties of two unexplored ternary copper phosphide materials. These are characterised by good performance, are based on abundant elements, have low gravimetric densities and good stability both in storage at room temperature and under temperature cycling in inert atmosphere. Further work on these materials and on related (copper) phosphides is of considerable interest. CaCuP has better overall electronic performance due to a better compromise between density of states effective mass (m_{DoS}^*), which dictates S and high carrier mobilities (μ), which largely controls ρ. To the best of our knowledge, CaCuP displays the largest reported S^2/ρ of any phosphide (barring the exceptional values resulting from the quantum thermoelectric Hall effect in TaP).[28] At 790 K both materials have κ_{lat} below 2 W m^{-1} K^{-1}, a promising result for compositions with no targeted alloying, suggesting that further improvements in zT can be achieved by atomic substitutions, processing and microstructure control. Currently both materials are over-doped and a method of controlling the p-type doping is required to maximise $S^2/\rho(T)$ and minimise $\kappa(T)$. Our data suggests that the p-type doping is linked to low levels of Cu vacancies in both materials, so control of doping would require minimisation of Cu vacancies. Future investigations need to examine the behaviour of vacancies with temperature. In addition, materials growth from slightly off-stoichiometric compositions is known to affect defect formation energies and should be explored. In the case of MgCuP, investigations of the hysteretic behaviour and n-type doping effects at high temperature are warranted. Combined with our recent report on the thermoelectric performance of CaAg$_{1-x}$P, we believe there is great unexplored potential within the large group of 1:1:1 ternary metal phosphides. From the materials reported here, CaCuP is the strongest contender, due to its better inherent electronic properties.

Conflicts of interest

There are no conflicts of interest to declare.

Notes and references

1 R. Funahashi, *Thermoelectric Energy Conversion*, Woodhead Publishing, 2021.
2 D. M. Rowe, *Materials, preparation, and characterization in thermoelectrics*, CRC Press, 2012.
3 J. H. Pohls, A. Faghaninia, G. Petretto, U. Aydemir, F. Ricci, G. D. Li, M. Wood, S. Ohno, G. Hautier, G. J. Snyder, G. M. Rignanese, A. Jain and M. A. White, *J. Mater. Chem. C*, 2017, **5**, 12441–12456.
4 J.-W. G. Bos, *Inorganic Thermoelectric Materials: From Fundamental Concepts to Materials Design*, The Royal Society of Chemistry, 2022, pp. 216–283, DOI: **10.1039/9781788019590-00216**.
5 J. Nuss, U. Wedig, W. Xie, P. Yordanov, J. Bruin, R. Hübner, A. Weidenkaff and H. Takagi, *Chem. Mater.*, 2017, **29**, 6956–6965.
6 A. Suwardi, L. Hu, X. Z. Wang, X. Y. Tan, D. V. M. Repaka, L. M. Wong, X. P. Ni, W. H. Liew, S. H. Lim, Q. Y. Yan, J. W. Xu, Y. Zheng and K. Hippalgaonkar, *ACS Appl. Mater. Interfaces*, 2020, **12**, 9150–9157.
7 V. Ponnambalam, S. Lindsey, W. Xie, D. Thompson, F. Drymiotis and T. M. Tritt, *J. Phys. D: Appl. Phys.*, 2011, **44**, 155406.
8 V. Ponnambalam and D. T. Morelli, *J. Electron. Mater.*, 2014, **43**, 1875–1880.
9 J. H. Pohls, S. Chanakian, J. Park, A. M. Ganose, A. Dunn, N. Friesen, A. Bhattacharya, B. Hogan, S. Bux, A. Jain, A. Mar and A. Zevalkink, *Mater. Horiz.*, 2021, **8**, 209–215.
10 J. Wang, O. I. Lebedev, K. Lee, J.-A. Dolyniuk, P. Klavins, S. Bux and K. Kovnir, *Chem. Sci.*, 2017, **8**, 8030–8038.
11 J. Mark and T. Mori, *ACS Appl. Energy Mater.*, 2021, **4**, 4861–4866.
12 K. Masumoto and S. Isomura, *Energy Convers.*, 1970, **10**, 129–133.
13 L. Fan, K. Peng, Z. Zhou, Y. Yan, C. Ran, H. Wang, G. Han, B. Zhang, X. Lu, G. Wang and X. Zhou, *Chem. Mater.*, 2022, **34**, 1620–1626.
14 R. J. Quinn and J.-W. G. Bos, *Appl. Phys. Lett.*, 2022, **120**, 073903.
15 A. Mewis, *Z. Naturforsch., B: Anorg. Chem., Org. Chem.*, 1979, **34**, 1373–1376.
16 A. Mewis, *Z. Naturforsch., B: Anorg. Chem., Org. Chem.*, 1978, **33**, 983–986.
17 B. A. D. Williamson, J. Buckeridge, J. Brown, S. Ansbro, R. G. Palgrave and D. O. Scanlon, *Chem. Mater.*, 2017, **29**, 2402–2413.
18 A. Mewis, *Z. Naturforsch., B: Anorg. Chem., Org. Chem.*, 1980, **35**, 942–945.
19 G. J. Snyder and E. S. Toberer, *Nat. Mater.*, 2008, **7**, 105–114.
20 H. J. Goldsmid and J. W. Sharp, *J. Electron. Mater.*, 1999, **28**, 869–872.
21 Z. M. Gibbs, H.-S. Kim, H. Wang and G. J. Snyder, *Appl. Phys. Lett.*, 2015, **106**, 022112.
22 H.-S. Kim, Z. M. Gibbs, Y. Tang, H. Wang and G. J. Snyder, *APL Mater.*, 2015, **3**, 041506.
23 T. M. Tritt, *Thermal Conductivity*, Springer, New York, NY, 2004.
24 B. Yu, M. Zebarjadi, H. Wang, K. Lukas, H. Wang, D. Wang, C. Opeil, M. Dresselhaus, G. Chen and Z. Ren, *Nano Lett.*, 2012, **12**, 2077–2082.
25 J. Willis, I. Bravić, R. R. Schnepf, K. N. Heinselman, B. Monserrat, T. Unold, A. Zakutayev, D. O. Scanlon and A. Crovetto, *Chem. Sci.*, 2022, **13**, 5872–5883.
26 R. J. Quinn and J. W. G. Bos, *Mater. Adv.*, 2021, **2**, 6246–6266.
27 G. J. Snyder, A. H. Snyder, M. Wood, R. Gurunathan, B. H. Snyder and C. Niu, *Adv. Mater.*, 2020, **32**, 2001537.
28 F. Han, N. Andrejevic, T. Nguyen, V. Kozii, Q. T. Nguyen, T. Hogan, Z. Ding, R. Pablo-Pedro, S. Parjan, B. Skinner, A. Alatas, E. Alp, S. Chi, J. Fernandez-Baca, S. Huang, L. Fu and M. Li, *Nat. Commun.*, 2020, **11**, 6167.
29 J. Xu, F. Han, T.-T. Wang, L. R. Thoutam, S. E. Pate, M. Li, X. Zhang, Y.-L. Wang, R. Fotovat, U. Welp, X. Zhou, W.-K. Kwok, D. Y. Chung, M. G. Kanatzidis and Z.-L. Xiao, *Phys. Rev. X*, 2021, **11**, 041029.
30 R. J. Quinn, C. Stevens, H. Leong, A. D. Huxley and J.-W. G. Bos, Dataset for New sustainable ternary copper phosphide thermoelectrics, 2022, DOI: **10.17861/a1d722e2-f3bc-45b6-8504-8932b9ff1320**.